A Hybrid Modulation Technique for Voltage Regulation in LLC Converters in the Presence of Transformer Parasitic Capacitance

Simone Palazzo
University of Cassino and Southern Lazio
Cassino, Italy
simone.palazzo@unicas.it

Giovanni Busatto
University of Cassino and Southern Lazio
Cassino, Italy
busatto@unicas.it

Enzo de Santis
University of Cassino and Southern Lazio
Cassino, Italy
enzo.desantis@unicas.it

Roberto Giacomobono
University of Cassino and Southern Lazio
Cassino, Italy
roberto.giacomobono02@gmail.com

Dario Di Ruzza
Rete Ferroviaria Italiana S.p.A.
Roma, Italy
d.diruzza@rfi.it

Giuseppe Panariello
Rete Ferroviaria Italiana S.p.A.
Roma, Italy
g.panariello@rfi.it

2022 IEEE Energy Conversion Congress and Exposition (ECCE) | 978-1-7281-9387-8/22/$31.00 ©2022 IEEE | DOI: 10.1109/ECCE50734.2022.9947909

***Abstract*— This work proposes a Hybrid Pulse Frequency-Phase Shift Modulation technique to solve the problem of voltage regulation in LLC converters when the transformer has a considerable stray capacitance. The generalized analytical model based on First Harmonic Approximation considering this stray capacitance is provided for the first time and its effects on the converter behavior are explained. Simulation results are presented to describe the operating principle of the modulation technique and the experimental validation is performed on a 2.5 kW LLC converter prototype.**

Keywords—parasitic capacitance, LLC converter, hybrid modulation technique, LLC modeling

I. INTRODUCTION

Among resonant converters, the LLC topology is by far the preferred solution for DC-DC conversion in many industrial applications such as electric vehicle chargers, telecom and servers power supplies, photovoltaic systems and adaptors, thanks to their wide regulation range, simple modulation technique and galvanic isolation [1]. Furthermore, thanks to the continuous development of SiC and GaN wide band-gap (WBG) power devices, it has been possible to increase the switching frequency, achieving optimal performances also in terms of efficiency and power density [1], [2], [3].

The research activity on these converters ranges from the development of optimal modulation techniques [4], [5], the study of the parasitic elements' effects on converter performances [3], [6]-[8], the implementation of the Soft Start-up [9], [10], the development of interleaved topologies for high power applications [11]-[13], the optimization of the magnetics [14], [15] and the reliability of power devices [1]. Among the various parameters, the parasitic capacitance of the transformer has a crucial importance because its presence has a major impact in LLC voltage regulation [3], [7]. The use of planar transformers (PTs) has become widely spread in isolated power converters in all the applications requiring high power density and high efficiency. One of the peculiar characteristics of PTs is the possibility of obtaining a very good coupling between windings with very reduced leakage inductances and resistances. Moreover, other features such as low profile, manufacturing repeatability and EMI reduction, make PTs by far the preferred solution in industrial applications [1], [6], [7]. However, despite these advantages, PTs also have greater inter-winding and intra-winding capacitances, depending on the number of the layers and the windings, the distance among them, the type of winding arrangement [16]-[18]. The reduction of this stray capacitance requires both technical and technological efforts to optimize the design of the transformer, causing a significant increase of the costs, making these solutions unpractical in many industrial applications, for which the stray capacitances are in the range 1–10 nF [2], [10], [14]. Moreover, the analytical model of parasitic capacitance is very complex and changes depending on numerous factors and, for this reason, it is almost always neglected when designing the converter, bringing to discrepancies between the experimental results and the expected theoretical behavior [2], [3], [15].

This work proposes the use of a hybrid modulation technique [4], [5], [19] to solve the problem of the voltage regulation in LLC converters for light loads and no-load in presence of the transformer stray capacitance. In Section II a generalized analytical model based on First Harmonic Approximation (FHA) [20] including the effects of parasitic capacitance of the transformer is presented for the first time. Moreover, in Section III the hybrid Pulse Frequency–Phase Shift Modulation technique (PFPSM) is proposed to solve the problem of the voltage regulation in LLC converters in the presence of a significant transformer stray capacitance. The control scheme of the hybrid modulation technique is described and validated with Simulink simulations. Finally, the experimental results obtained on a 2.5 kW LLC converter prototype are provided in Section IV and the conclusion is in Section V.

II. GENERALIZED ANALYTICAL MODEL FOR LLC CONVERTER

The theoretical equivalent model of a transformer including all its parasitic components is supplied in many papers [3], [7], [12], [17] and one of the proposed equivalent circuit is shown in Fig. 1 (a), where the series leakage resistance and inductance for both primary and secondary side are considered, respectively R_{Lk1}, L_{Lk1}, R_{Lk2} and L_{Lk2}. The parasitic intrawinding (C_{12}, C_{34}) and interwinding (C_{13}, C_{14}, C_{23}, C_{24}) capacitances are also shown to represent the effect of the distributed capacitances between the turns and the windings of the transformer. Neglecting the interwinding capacitances, whose value is much smaller than the intrawinding ones, and reporting to the primary side the other

978-1-7281-9387-8/22/$31.00 ©2022 IEEE

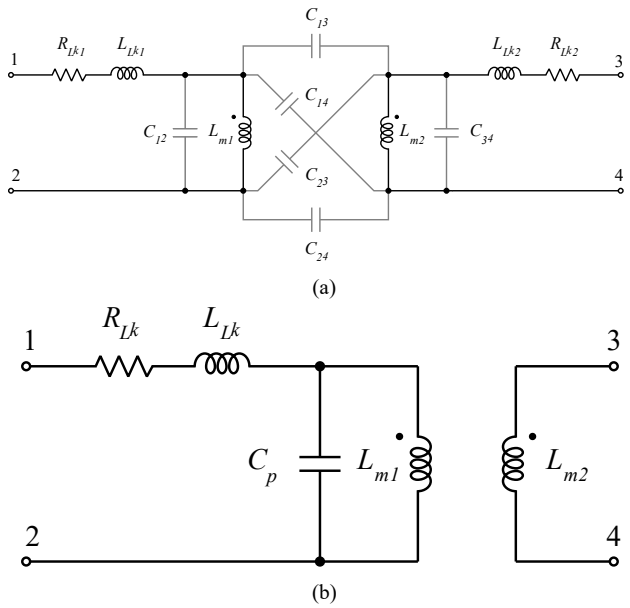

Fig. 1. (a) Equivalent circuit of the transformer including the parasitic capacitances; (b) Simplified equivalent circuit of the transformer considering only an equivalent parasitic capacitance.

parasitic elements, it is possible to derive the equivalent circuit of Fig. 1 (b), that includes the effects of the intrawinding capacitances in the capacitor C_p. This equivalent circuit is used for the transformer in the generalized analytic model of the LLC converter.

Fig. 2 depicts the circuit schematic of an LLC converter in full bridge configuration for the primary side and a full-wave rectifier for the secondary side, where the transformer is modeled by its magnetizing inductance L_m and stray capacitance C_p. The resistance R_p accounts for the winding parasitic resistance of the transformer, the *on*-resistance of the power devices and the PCB tracks. The leakage inductance of the transformer is placed in series with the resonant inductor L_r, hence its effect can be directly incorporated in L_r and it is not shown.

According to the FHA [20], it is possible to derive the following equation in Laplace domain:

$$\frac{V_o(s)}{V_i(s)} = \frac{Z_2(s)}{Z_1(s) + Z_2(s)} \tag{1}$$

Where:

$$Z_1(s) = \frac{s^2 L_r C_r + s R_p C_r + 1}{s C_r} \tag{2}$$

$$Z_2(s) = \frac{s L_m R_{ac}}{s^2 L_m C_p R_{ac} + s L_m + R_{ac}} \tag{3}$$

In (2) and (3), C_r is the resonant capacitor and R_{ac} is the equivalent load resistance reflected to the primary side of the transformer, equal to $8n^2 R_o/\pi^2$, with R_o representing the load resistance and n the transformer turn ratio [20]. Writing $Z_1(s)$ and $Z_2(s)$ as the ratio of two polynomials, such that

$$Z_1(s) = \frac{N_1(s)}{D_1(s)} \tag{4}$$

$$Z_2(s) = \frac{N_2(s)}{D_2(s)} \tag{5}$$

Eq. (1) becomes:

$$\frac{V_o(s)}{V_i(s)} = \frac{N_2(s) D_1(s)}{N_1(s) D_2(s) + N_2(s) D_1(s)} =$$

$$= \frac{s^2 L_m C_r R_{ac}}{\left(s^2 L_r C_r + s R_p C_r + 1\right)\left(s^2 L_m C_p R_{ac} + s L_m + R_{ac}\right) + s^2 L_m C_r R_{ac}} \tag{6}$$

Putting in evidence the terms L_m, C_r, R_{ac}, eq. (6) can be rewritten as:

$$\frac{V_o(s)}{V_i(s)} = \\ = \frac{s^2 m}{\left(s^2 + s\frac{R_p}{L_r} + \omega_r^2\right)\left(\frac{s^2}{\omega_p^2} + s\frac{L_m}{R_{ac}} + 1\right) + s^2 m} \tag{7}$$

The definition of the parameters is provided in Table I.

TABLE I. PARAMETERS FOR THE LLC MODEL

Symbol	Definition
$\omega_r = \frac{1}{\sqrt{L_r C_r}}$	Series resonance angular frequency
$\omega_p = \frac{1}{\sqrt{L_m C_p}}$	Parallel resonance angular frequency
$\omega_z = \frac{\omega_p}{\omega_r}$	Angular frequency ratio
$m = \frac{L_m}{L_r}$	Inductance ratio
$Q = \frac{\omega_r L_r}{R_{ac}}$	Ideal quality factor
$Q_p = \frac{\omega_r L_r}{R_p}$	Parasitic quality factor

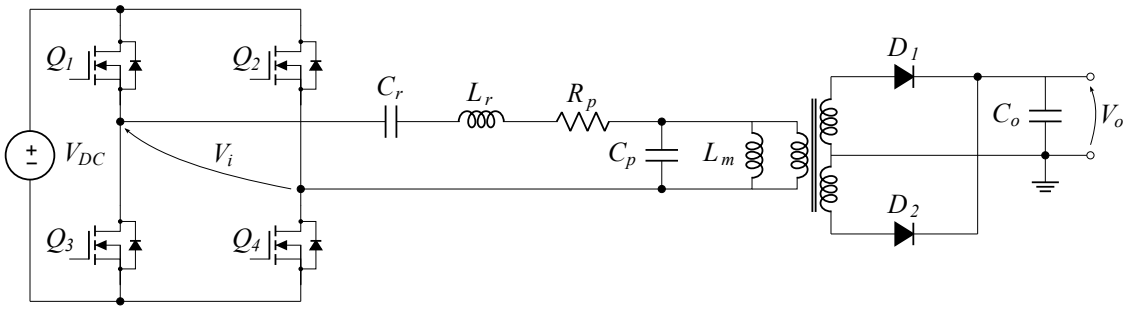

Fig. 2. Circuit scheme of an LLC converter with simplified equivalent model of the transformer and parasitic resistance.

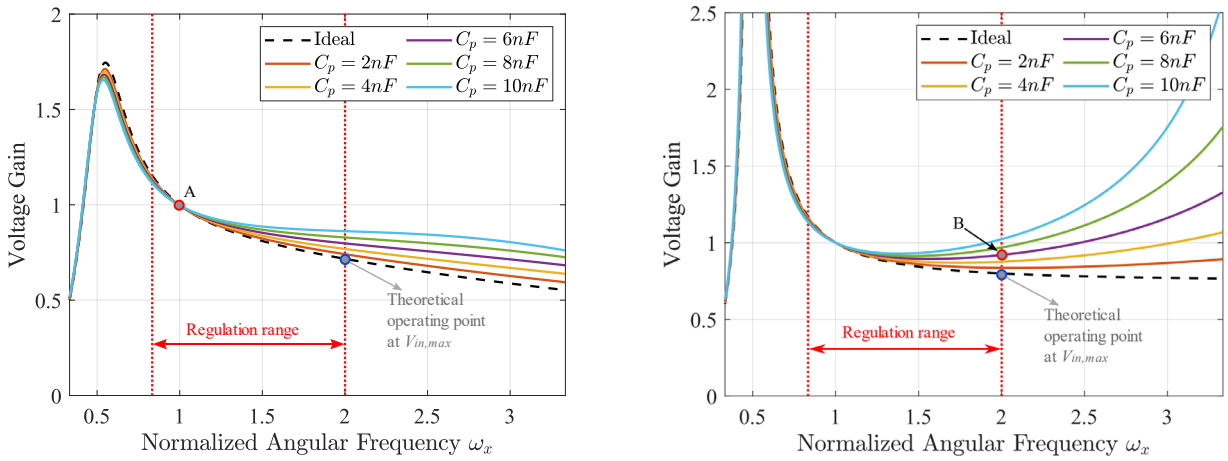

Fig. 3. Voltage gain characteristic vs normalized angular frequency, coinciding with switching frequency, derived from the FHA analysis for different values of C_p: (a) for 2.5kW nominal load; (b) for 100W load.

Now, limiting the analysis to the frequency domain, setting $s = j\omega$, putting in evidence the term ω_r^2 in the denominator and knowing that

$$\frac{L_m}{R_{ac}} = \frac{mQ}{\omega_r} \tag{8}$$

it is possible to derive the final equation for the voltage gain of the LLC converter including the parasitic elements C_p and R_p:

$$\frac{V_o(j\omega)}{V_i(j\omega)} = \\ = \frac{1}{1 - \left(\frac{1-\omega_x^2}{m\omega_x^2} + j\frac{1}{mQ_p\omega_x}\right)\left(1 - \left(\frac{\omega_x}{\omega_z}\right)^2 + jmQ\omega_x\right)} \tag{9}$$

where:

$$\omega_x = \frac{\omega}{\omega_r} \tag{10}$$

represents the normalized angular frequency. It is worth to note that the ideal equation for the voltage gain without parasitic elements can be easily derived from this equation, considering that when R_p and C_p tend to 0, both Q_p and ω_z tend to $+\infty$, bringing to:

$$\frac{V_o(j\omega)}{V_i(j\omega)} = \frac{1}{1 - \left(\frac{1-\omega_x^2}{m\omega_x^2}\right)(1 + jmQ\omega_x)} \tag{11}$$

Fig. 3 shows the voltage gain curve vs the normalized angular frequency ω_x for different values of C_p for nominal load, 2.5 kW (a) and for 100 W load, (b). It is evident that the presence of the stray capacitance significantly affects the gain for frequencies larger than the resonance frequency. This effect is observed in all load conditions, but it becomes very important at light loads, at which the converter exhibits a step-up behavior where it is requested to be a step-down. Consequently, the switching frequency can no longer be used to regulate the output voltage causing the control to fail and the output voltage to be uncontrolled. The gain curves of Fig. 3 evidence that at light loads, because of the stray capacitances, the LLC becomes an LCC operated below the resonance frequency and then causing the power devices to be switched on a capacitive load.

III. The Hybrid Pulse Frequency – Phase Shift Modulation Technique

Hybrid Modulation Techniques are presented in the literature for different types of industrial applications [4], [5], but they have never been used to mitigate the problems of the voltage regulation in LLC converters due to the stray capacitance. The PFPSM, proposed in this work, automatically splits from one type of modulation to the other to regulate the output voltage for all operating conditions even in the presence of considerable stray capacitances. Moreover, this modulation technique can also simplify the converter soft start-up avoiding the problems associated with the frequency control during the start-up [9], [10], [19].

A. PFPSM logic

The control block diagram of the PFPSM is shown in Fig. 4, where a classic single closed loop control is used. The output voltage error E_v is computed as the difference between the reference voltage $V_{o,ref}$ and the measured output voltage $V_{o,m}$, that also considers the transducer factor K_v. Two different control networks are used to manage the regulation and both controllers make use of PI regulators, which can be easily implemented in a digital microcontroller.

The output control variables for PFM and PSM are the switching frequency f_s and the phase shift ϕ_s between the two legs of the primary full bridge, respectively. Each state is characterized by the general control status output $x_k = [f_{s_k}, \phi_{s_k}]$, where k defines a specific status. The duty cycle is

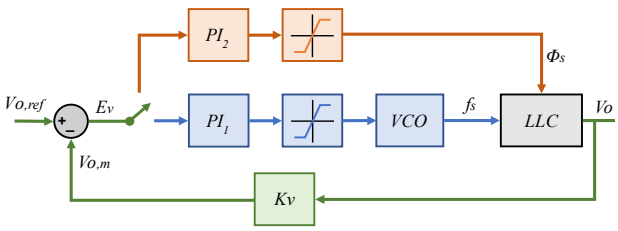

Fig. 4. Control scheme for the proposed PFPSM. The control network related to PFM is depicted in blue, while the PSM one is highlighted in orange.

always set to 50% and the deadtime is varied according to the law

$$\mathrm{DT}(f_s) = \frac{\delta}{f_s} \tag{12}$$

where δ represents a constant defining the percentage of the deadtime with respect the switching period. It is possible to use other optimized but more complicated strategies of deadtime variation, as in [21], in order to improve the switching behavior of the power devices, but it has no impact on the proposed modulation strategy.

The logic of the proposed control technique is described through the flow chart of Fig. 5. During the soft-start, the control status is set to $x_1 = [f_{s_{max}}, 0°]$ and the phase shift is linearly increased until it reaches 180°, maintaining constant f_s to $f_{s_{max}}$. After the soft-start phase, the converter operates in PFM with a variable switching frequency and 180° fixed phase-shift, so the control status is $x_2 = [f_s, 180°]$. PFM is always preferred when it permits the output voltage regulation. However, depending on the operating conditions, it may be necessary to switch from PFM to PSM. This happens if the switching frequency is above the threshold $f_{s,th}$ and the output voltage error E_v is lower than the minimum negative error threshold $-E_v^*$, or if a sudden variation of the load or the input voltage causes the error E_v to be lower than a maximum admissible negative value $-E_{v,Max}$. In this case PSM acts to decrease the output voltage by reducing ϕ_s until the error tends to zero. Thus, the output control status is $x_3 = [\overline{f_s}, \phi_s]$, where $\overline{f_s}$ indicates the fixed frequency value defined by the previous state of PFM. The threshold frequency $f_{s,th}$ can be chosen from the analytical curves derived with FHA in order to avoid capacitive regions of the gain characteristic, that would badly affect the switching of the power devices. The described modulation logic ensures the continuity of the state variables f_s and ϕ_s even if there are two different control networks. The stability of the whole system can be affected by the change from one status to another, but this topic is outside the scope of this paper and will be studied later.

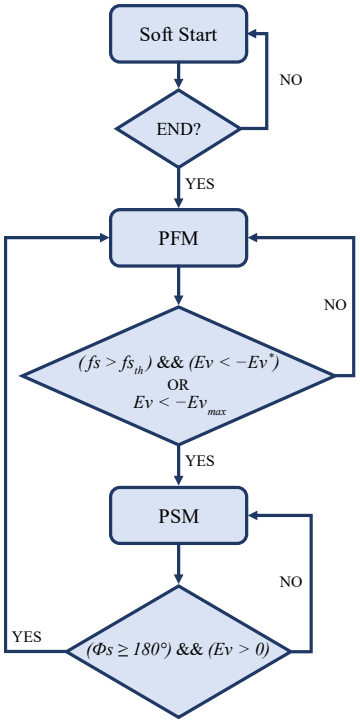

Fig. 5. Flow chart of the proposed Hybrid PFPS Modulation Technique.

B. *Simulation analysis*

Simulink simulations were performed for a 2.5kW – 144V LLC converter, considering a 6 nF stray capacitance of the transformer. The values of all the parameters used in the simulation are shown in Tab. II.

TABLE II. PARAMETERS FOR THE SIMULATION ANALYSIS

Parameter	Value	Parameter	Value
V_{DC}	300 V ± 10%	L_m	48 µH
V_o	144 V	L_r	16 µH
P_o	2.5 kW	C_r	110 nF
f_r	120 kHz	C_o	110 µF
f_s	80 – 190kHz	C_p	6 nF
n	2	R_p	0.1 Ω

As depicted in Fig. 6, a classic PFM would cause the output voltage to reach unacceptable values compared to the ideal case for 1% of nominal load.

The standard solution in this case would be the operation of the converter in burst mode, during which the gate driver signals are kept low when the output voltage exceeds a defined maximum value $V_{o,max}$, causing the output capacitor to be partially discharged. Then, when the capacitor is discharged under a minimum threshold $V_{o,min}$, the switches are turned-on again and the output voltage increases consequently. This solution makes the voltage oscillates between $V_{o,max}$ and $V_{o,min}$ in order to obtain the desired output voltage as its mean value. The waveform of the output voltage during this operation is reported in yellow in Fig. 6. This solution causes a high current stress on the output capacitor and the power devices, also bringing to higher losses and EMI issues [22].

On the contrary, the proposed PFPSM achieves perfect regulation of the output voltage even for a step load variation from 100% to 1%, as shown in Fig. 7 (a), where the three

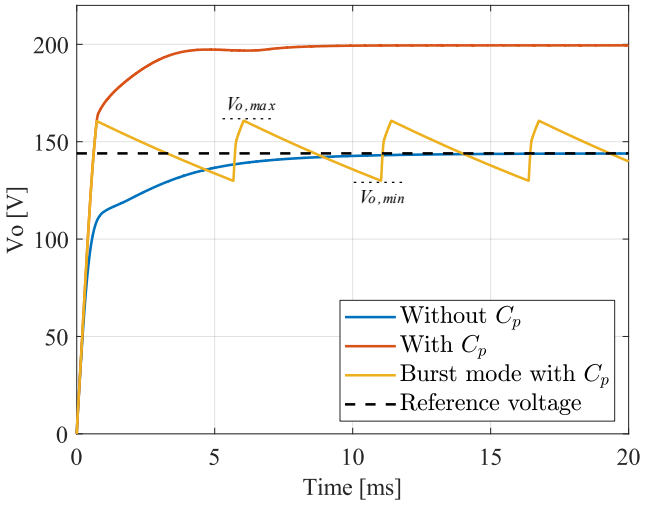

Fig. 6. Output voltage evolution with only PFM for 1% of nominal load.

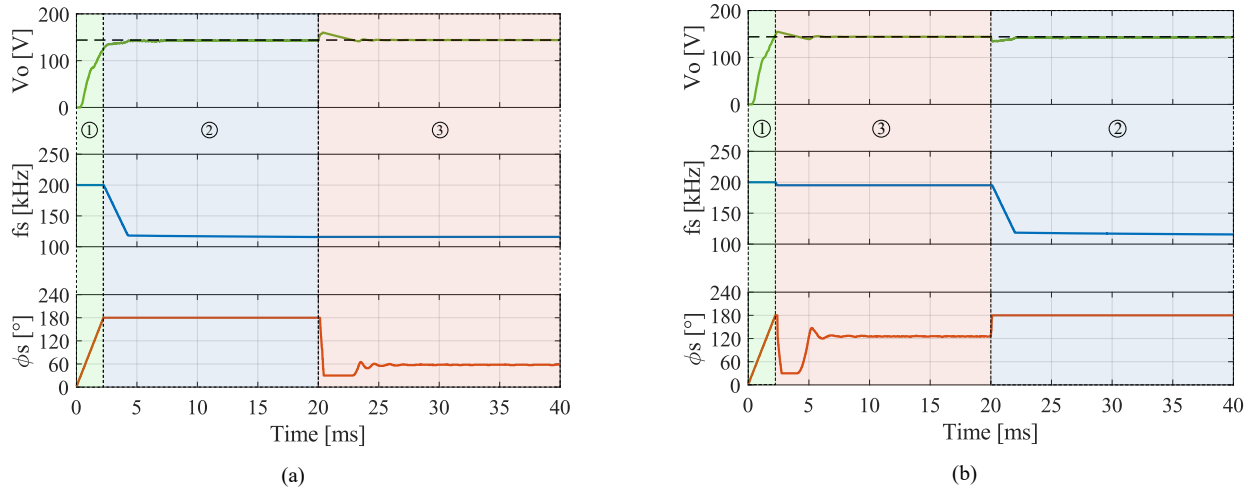

(a) (b)

Fig. 7. Operation of the proposed PFPSM for different load conditions: (a) Step load variation from 100% to 1% of nominal load after 20 ms; (b) Step load variation from 1% to 100% of nominal load after 20 ms. The highlighted operation regions are: ① Soft-start (green), ② PFM operation (blue), ③ PSM operation (red).

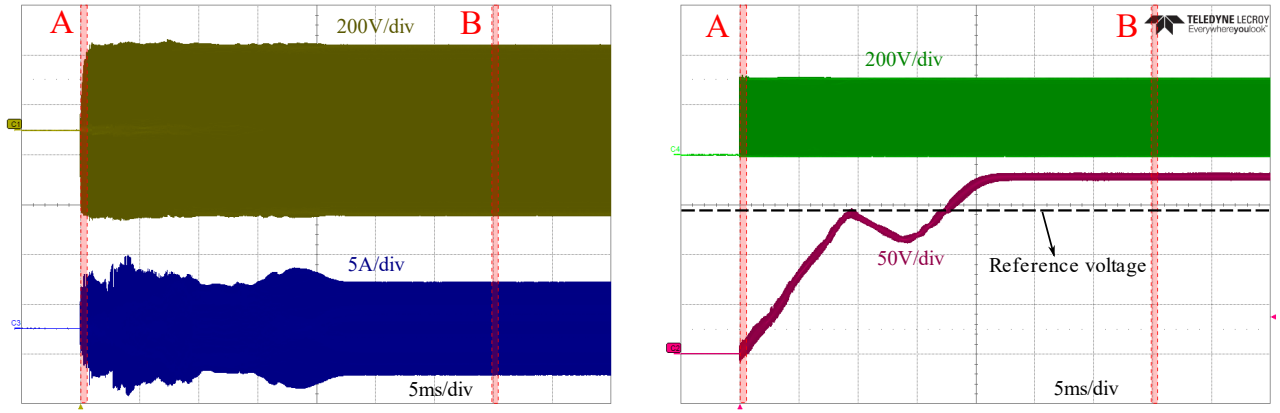

Fig. 8. Experimental waveforms with PFM of primary side transformer voltage (yellow) and current (blue), drain-to-source voltage (green) and output voltage (red) for V_{in} = 300 V, P_{out} = 100 W.

different operation regions of the modulation technique are highlighted.

To underline the outstanding dynamic performances of this control technique, Fig. 7 (b) shows the simulated output voltage and control signals starting from a load condition of 1% of the nominal load. In this case, after the soft start-up of the converter, the output voltage would reach a value much higher than the reference, but the phase shift ϕ_s quickly decreases when the computed voltage error overcomes the imposed limit and, after a settling time, it is brought to zero, achieving a perfect regulation. After 20 ms, a step load variation from 1% to 100% of the nominal load is performed, the phase shift ϕ_s immediately increases up to 180° and the control logic switches to PFM, achieving a perfect regulation of the output voltage also in this case.

IV. Experimental Results

A 2.5 kW, 300 V input and 144 V output LLC converter prototype has been constructed, using 600 V–75 A CoolMOS technology MOSFETs for the primary bridge, 650 V–50 A SiC Schottky diodes for the rectifier and a planar transformer with turn ratio 2. The parasitic capacitance of the transformer measured with an impedance analyzer is 6 nF.

Different experimental tests have been performed to show the limitations of PFM in regulating the voltage at light load and the benefits of using the hybrid PFPSM, not only for the regulation in this load condition, but also during the soft start-up of the converter. In all the tests, the soft start-up was implemented by using the PSM, in order to limit the current peak at the start-up of the converter, reducing the stress on the transformer, the power devices and the capacitors [19].

In the first test PSM was used only during the start-up phase while PFM was used in steady state. Fig. 8 shows the waveforms at the converter turn-on of current and voltage at the transformer primary side, drain-to-source voltage of Q_1 switch and output voltage. The test conditions are: V_{in} = 300 V, P_{out} = 100 W. As the reader can see, the steady state value of the output voltage is larger than the reference voltage of 144 V and reaches 170 V. To correct this problem, if we consider the ideal frequency–voltage gain of an LLC (see Fig. 3 (a)), in principle, we should increase the switching frequency. Instead, because of the parasitic capacitance of the transformer, the converter behaves like an LCC in these test conditions (see Fig. 3 (b)) and the increase of the frequency would result in a further increase of the voltage. Consequently, the control logic is not able to regulate the output voltage because it forces the switching frequency to the maximum value (190 kHz) and causes the voltage to reach the value predicted by the gain voltage curve at that frequency. To better

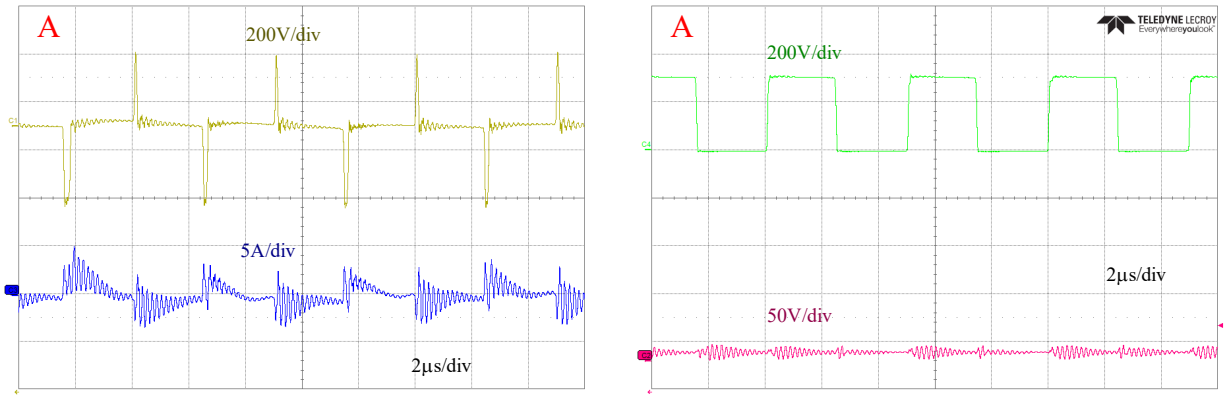

(a)

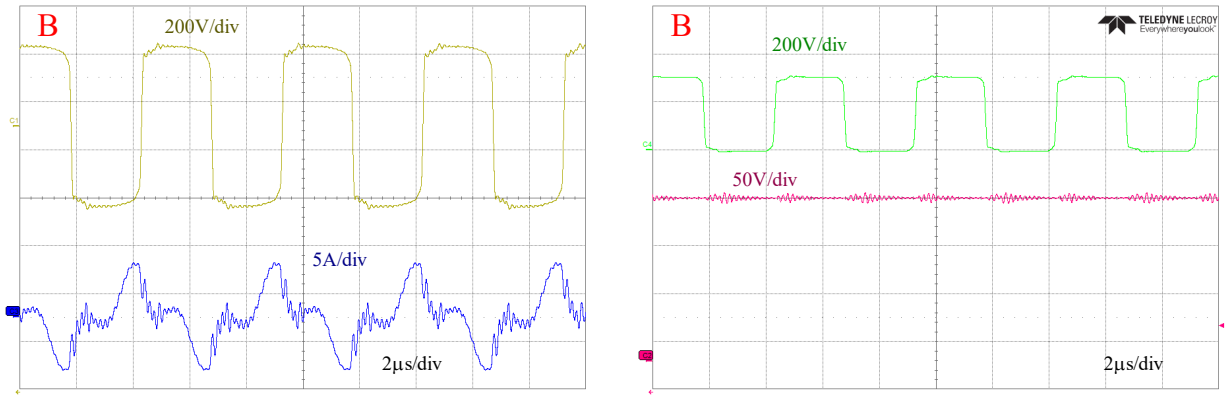

(b)

Fig. 9. Details of the experimental waveforms of Fig. 8: (a) start-up phase of the converter with PSM; (b) steady state operation with PFM. The waveforms are: transformer voltage (yellow) and current (blue), drain-to-source voltage (green) and output voltage (red). The test conditions are V_{in} = 300 V, P_{out} = 100 W.

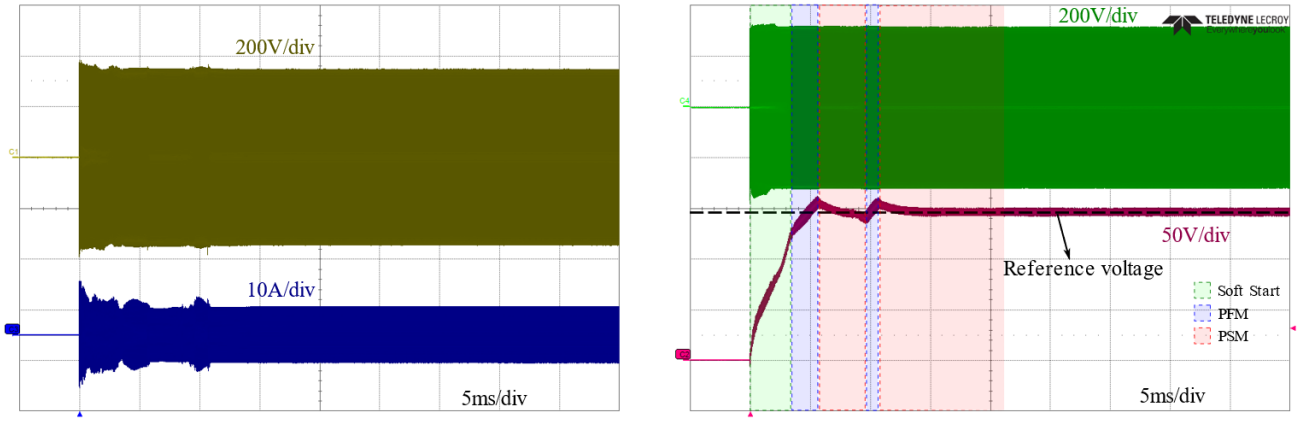

Fig. 10. Experimental waveforms with PFPSM of primary side transformer voltage (yellow) and current (blue), output voltage of the full-bridge (green) and output voltage (red) for V_{in} = 300 V, P_{out} = 100 W.

understand the operations of the converter, Fig. 9 shows the zooms in the two highlighted areas of Fig. 8. In particular Fig. 9 (a) depicts the waveforms during the start-up phase of the converter, that is performed in PSM with a 190 kHz fixed switching frequency (region A). Looking at the transformer voltage, the reader can note the very short energizing phases each of which causes a very small increase of the current. For the largest part of the switching period, the converter operates in free-wheeling mode. The parasitic inductance and the parasitic capacitances of transformer and rectifier diodes cause the resonant oscillations of current and voltage.

Along the start-up phase, the phase shift between the two legs is progressively increased together with the duration of the energizing phases. The PFM starts when the phase shift reaches 180°. Fig. 9 (b) shows the zoom in steady state (region B), where PFM is used for the regulation. It is worth noting that the switching frequency is 190 kHz (maximum frequency) and the MOSFETs of the primary bridge are still soft switched.

On the contrary, the output voltage can be easily regulated when using the hybrid PFPSM, even at light load conditions. As an example, Fig. 10 shows the waveforms of transformer voltage and current, output voltage of the full-bridge and output voltage in the same previous test conditions, i.e. V_{in} = 300 V, P_{out} = 100 W. In this case, after the soft start-up (green region), similar to that of Fig. 8, the control logic starts

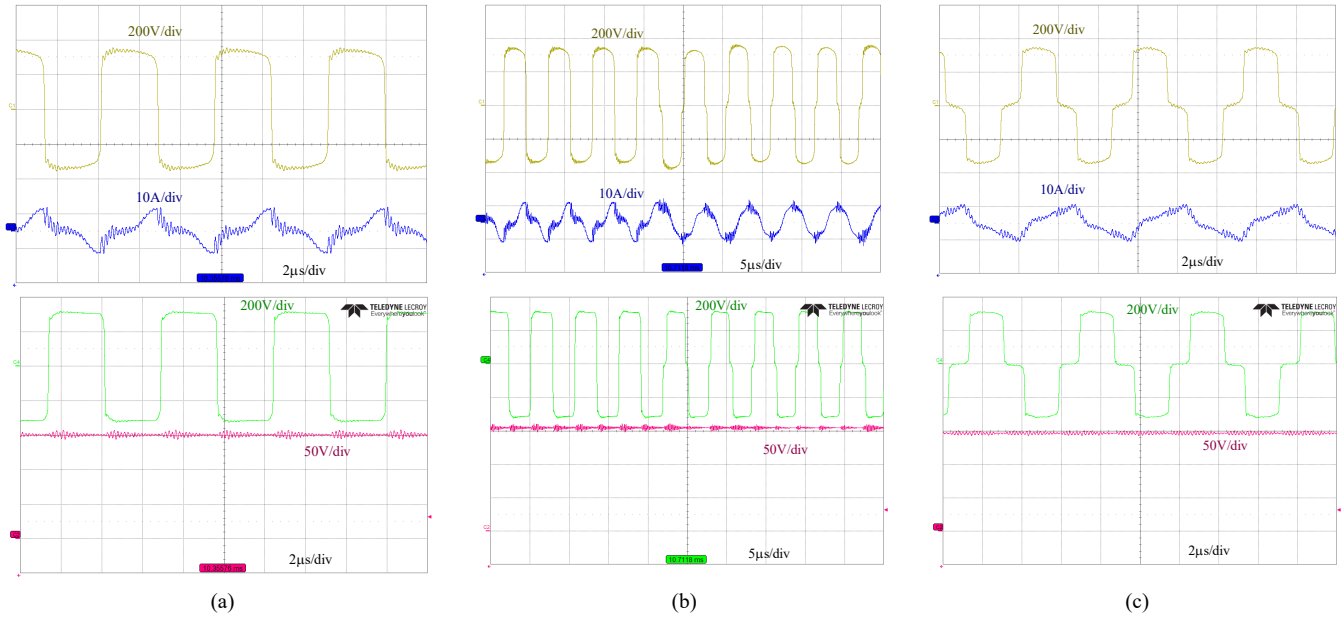

(a) (b) (c)

Fig. 11. Operation of LLC converter with PFPSM: (a) during PFM; (b) transition between PFM and PSM; (c) during PSM in steady state. The waveforms are transformer voltage (yellow) and current (blue), output voltage of the full-bridge (green) and output voltage (red), for V_{in} = 300 V, P_{out} = 100 W.

with PFM (blue region) trying to regulate the output voltage by increasing the switching frequency towards the maximum value. When the error overcomes the predefined threshold, the control switches to PSM (red region), hence the switching frequency remains to its maximum value and the output voltage is regulated by reducing the phase shift between the two legs of the primary bridge until the output voltage error tends to zero.

Fig. 11 shows the detailed waveforms during the operation of the LLC converter with PFPSM, highlighting the PFM region (a), the transition between PFM and PSM (b) and the steady state operation in PSM (c). Although the output voltage regulation is achieved, the effects of the parasitic capacitance can be easily recognized in the superimposed high frequency oscillations in the transformer current. It is worth noting that the MOSFETs of the primary bridge are soft switched in all conditions.

The regulation is achieved with PFPSM technique even at no load conditions when a voltage error less than 8 V (5% of nominal voltage) is measured as depicted in Fig. 12 (a), where the waveforms of transformer voltage and current, the output voltage of the full-bridge and the output voltage are shown for V_{in} = 300 V and P_{out} = 8 W, corresponding to 0.3% of the rated power. This power is dissipated on the ballast resistor of 2.6 kΩ used to avoid the complete absence of load. For comparison, Fig. 12 (b) reports the waveforms registered in the same test conditions but with a PFM control in steady state. In this latter case the output voltage tends to about 250 V as expected for an LCC converter at such a low load.

An extended experimental characterization of the converter, whose results are not reported here for brevity, has shown that the proposed control logic allows the regulation of the output voltage in all load conditions and, at the same time, it ensures the LLC operation in a wide range of loads.

V. Conclusion

This work proposes a hybrid PFPSM technique to solve the problems of the voltage regulation related to the transformer parasitic capacitance in the LLC converter, that has a relevant impact especially when using planar technology for the transformer. The analytical model based on FHA has been improved considering also the presence of the parasitic capacitance and resistance and their effects on voltage regulation are presented and explained. The logic of the hybrid modulation technique is described and its performances in regulating the voltage are compared to the standard PFM and the burst-mode operation. Finally, the developed PFPSM technique has been tested on an LLC converter prototype, achieving a good regulation even at no load conditions.

Acknowledgment

This work has been supported partially by the project "HEROGRIDS – Holistic approach to EneRgy-efficient smart nanOGRIDS" funded by the MIUR Progetti di Ricerca di Rilevante Interesse Nazionale (PRIN) Bando 2017 - grant 2017WA5ZT3_001, and partially by MIUR in the mainframe of the program "Dipartimenti Universitari di Eccellenza, 2018-2022. Area 09" under Law 232, December, 11th 2016.

References

[1] S.A. Mortazavizadeh, S. Palazzo, A. Amendola, E. de Santis, D. Di Ruzza, G. Panariello, A. Sanseverino, F. Velardi and G. Busatto, "High Frequency, High Efficiency, and High Power Density GaN-Based LLC Resonant Converter: State-of-the-Art and Perspectives". Appl. Sci. 2021, 11, 11350.

[2] S. Ann, W. -J. Son, J. H. Lee, J. Byun and B. K. Lee, "Design of a SiC-based LLC Resonant Converter for On-Board Chargers Considering Parasitic Capacitance of Planar Transformer," 2020 23rd International Conference on Electrical Machines and Systems (ICEMS), 2020, pp. 315-319, doi: 10.23919/ICEMS50442.2020.9291245.

[3] M. A. Saket, N. Shafiei and M. Ordonez, "LLC Converters With Planar Transformers: Issues and Mitigation," in IEEE Transactions on Power Electronics, vol. 32, no. 6, pp. 4524-4542, June 2017, doi: 10.1109/TPEL.2016.2602360.

[4] Y. Wei, Q. Luo and A. Mantooth, "Overview of Modulation Strategies for LLC Resonant Converter," in IEEE Transactions on Power Electronics, vol. 35, no. 10, pp. 10423-10443, Oct. 2020, doi: 10.1109/TPEL.2020.2975392.

[5] B. McDonald and F. Wang, "LLC performance enhancements with frequency and phase shift modulation control," 2014 IEEE Applied Power Electronics Conference and Exposition - APEC 2014, 2014, pp. 2036-2040, doi: 10.1109/APEC.2014.6803586.

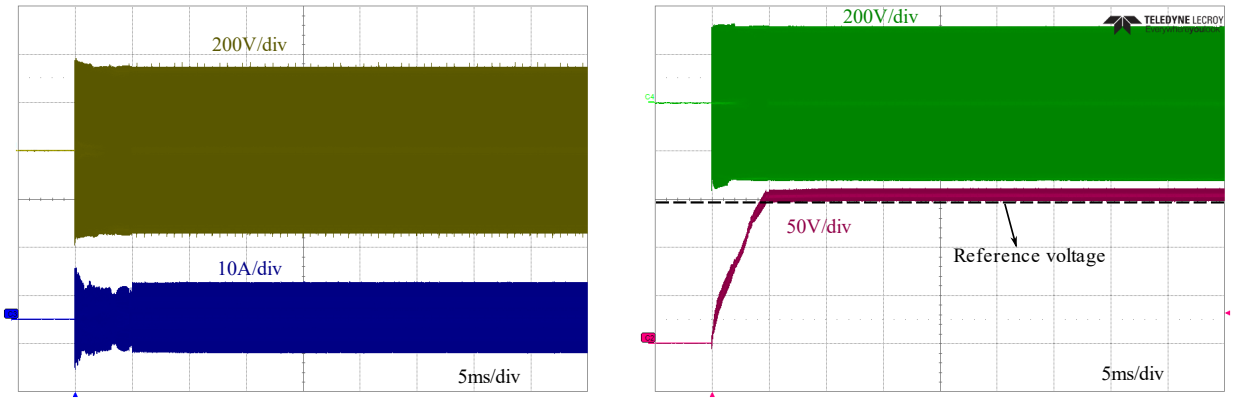

(a)

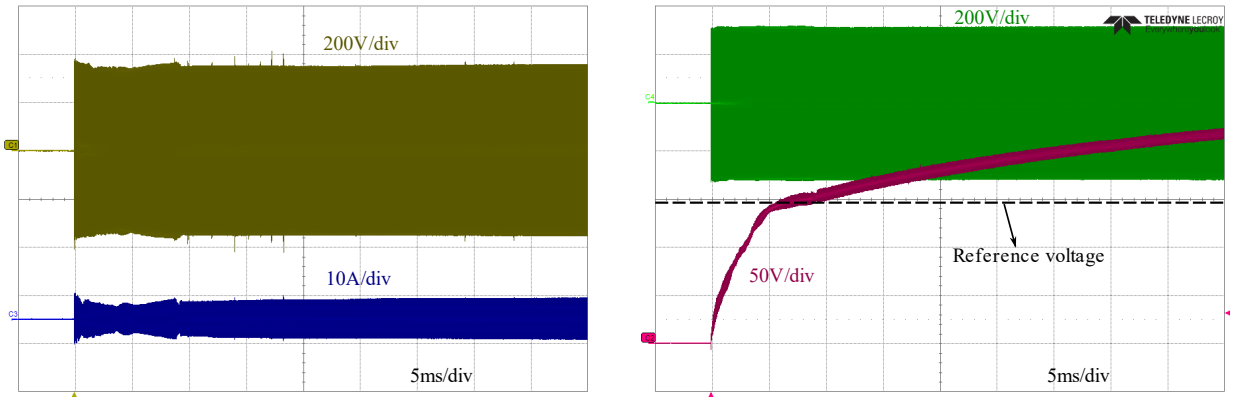

(b)

Fig. 12. Experimental waveforms of primary side transformer voltage (yellow) and current (blue), output voltage of the full-bridge (green) and output voltage (red) when: (a) PSM and (b) PFM are used in steady state. The test conditions are: V_{in} = 300 V, P_{out} = 8 W.

[6] Li, F.; Hao, R.; Lei, H.; Zhang, X.; You, X. "The Influence of Parasitic Components on LLC Resonant Converter". Energies 2019, 12, 4305. https://doi.org/10.3390/en12224305.

[7] L. Deng, P. Wang, X. Li, H. Xiao and T. Peng, "Investigation on the Parasitic Capacitance of High Frequency and High Voltage Transformers of Multi-Section Windings," in IEEE Access, vol. 8, pp. 14065-14073, 2020, doi: 10.1109/ACCESS.2020.2966496.

[8] H. Chen and X. Wu, "Analysis on the influence of the secondary parasitic capacitance to ZVS transient in LLC resonant converter," 2014 IEEE Energy Conversion Congress and Exposition (ECCE), 2014, pp. 4755-4760, doi: 10.1109/ECCE.2014.6954052.

[9] C. Fei, F. C. Lee and Q. Li, "Digital Implementation of Soft Start-Up and Short-Circuit Protection for High-Frequency LLC Converters With Optimal Trajectory Control (OTC)," in IEEE Transactions on Power Electronics, vol. 32, no. 10, pp. 8008-8017, Oct. 2017, doi: 10.1109/TPEL.2016.2631467.

[10] W. Feng and F. C. Lee, "Optimal trajectory control of LLC resonant converters for soft start-up," 2013 Twenty-Eighth Annual IEEE Applied Power Electronics Conference and Exposition (APEC), 2013, pp. 1445-1451, doi: 10.1109/APEC.2013.6520488.

[11] T. Pereira, F. Hoffmann, R. Zhu and M. Liserre, "A Comprehensive Assessment of Multiwinding Transformer-Based DC–DC Converters," in IEEE Transactions on Power Electronics, vol. 36, no. 9, pp. 10020-10036, Sept. 2021, doi: 10.1109/TPEL.2021.3064302.

[12] L. F. Costa, G. Buticchi and M. Liserre, "Highly Efficient and Reliable SiC-Based DC–DC Converter for Smart Transformer," in IEEE Transactions on Industrial Electronics, vol. 64, no. 10, pp. 8383-8392, Oct. 2017, doi: 10.1109/TIE.2017.2696481.

[13] Y. Li, S. Shao, H. Chen, J. Zhang and K. Sheng, "High-gain high-efficiency IPOS LLC converter with coupled transformer and current sharing capability," in CPSS Transactions on Power Electronics and Applications, vol. 5, no. 1, pp. 63-73, March 2020, doi: 10.24295/CPSSTPEA.2020.00006.

[14] Z. Zhang, C. Liu, M. Wang, Y. Si, Y. Liu and Q. Lei, "High-Efficiency High-Power-Density CLLC Resonant Converter With Low-Stray-Capacitance and Well-Heat-Dissipated Planar Transformer for EV On-Board Charger," in IEEE Transactions on Power Electronics, vol. 35, no. 10, pp. 10831-10851, Oct. 2020, doi: 10.1109/TPEL.2020.2980313.

[15] Ouyang, Z., Thomsen, O. C., & Andersen, M. A. E. (2010). "Optimal Design and Tradeoffs Analysis for Planar Transformer in High Power DC-DC Converters". In The 2010 International Power Electronics Conference – ECCE ASIA - IPEC-Sapporo 2010 IEEE.

[16] M. A. Saket, N. Shafiei and M. Ordonez, "Planar transformer winding technique for reduced capacitance in LLC power converters," 2016 IEEE Energy Conversion Congress and Exposition (ECCE), 2016, pp. 1-6, doi: 10.1109/ECCE.2016.7855352.

[17] J. Biela and J. W. Kolar, "Using Transformer Parasitics for Resonant Converters—A Review of the Calculation of the Stray Capacitance of Transformers," in IEEE Trans. Ind. Appl., vol. 44, no. 1, 2008.

[18] R. Shafaei, M. C. G. Perez and M. Ordonez, "Planar Transformers in LLC Resonant Converters: High-Frequency Fringing Losses Modeling," in IEEE Transactions on Power Electronics, vol. 35, no. 9, pp. 9632-9649, Sept. 2020, doi: 10.1109/TPEL.2020.2971424.

[19] Y. Ling, Z. Guo and X. Liu, "The Soft-Start Analysis of a Full-Bridge LLC Converter with Hybrid Control Strategy," 2016 IEEE Vehicle Power and Propulsion Conference (VPPC), 2016, pp. 1-4, doi: 10.1109/VPPC.2016.7791801.

[20] S. De Simone, C. Adragna, C. Spini and G. Gattavari, "Design-oriented steady-state analysis of LLC resonant converters based on FHA," International Symposium on Power Electronics, Electrical Drives, Automation and Motion, 2006. SPEEDAM 2006., 2006, pp. 200-207, doi: 10.1109/SPEEDAM.2006.1649771.

[21] Y. Wei, Q. Luo, Z. Wang and H. Alan Mantooth, "Simple and Effective Adaptive Deadtime Strategies for LLC Resonant Converter: Analysis, Design, and Implementation," in IEEE Journal of Emerging and Selected Topics in Power Electronics, 2021, doi: 10.1109/JESTPE.2021.3058234.

[22] W. Jiang, J. Zhang, S. Shao, X. Wu and J. Zhang, "Constant Burst Frequency Control for LLC Converters with Trajectory Control," 2018 IEEE Energy Conversion Congress and Exposition (ECCE), 2018, pp. 6804-6808, doi: 10.1109/ECCE.2018.8557809.